

AD-A170 176

DYNAMIC FORMATION OF STRESSED CORONAL MAGNETIC FIELDS

1/1

(U) CALIFORNIA UNIV IRVINE DEPT OF PHYSICS

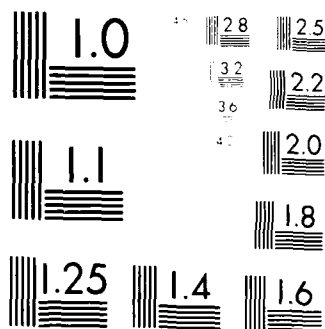
R S STEINOLFSON FEB 86 AFGL-TR-86-0062 F19628-85-K-0006

UNCLASSIFIED

F/G 3/2

NL





NATIONAL BUREAU OF STANDARDS
 4790
 1963

12

AFGL-TR-86-0062

Dynamic Formation of Stressed Coronal
Magnetic Fields

R. S. Steinolfson

University of California
Department of Physics
Irvine, CA 92717

February 1986

Final Report
2 November 1984 - 2 February 1986

APPROVED FOR PUBLIC RELEASE: DISTRIBUTION UNLIMITED

AIR FORCE GEOPHYSICS LABORATORY
AIR FORCE SYSTEMS COMMAND
UNITED STATES AIR FORCE
HANSCOM AIR FORCE BASE, MASSACHUSETTS 01731

DTIC
ELECTE
JUL 24 1986
S D

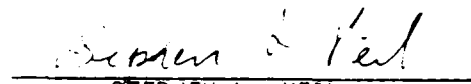
AD-A170 176

23 405

6 7

This technical report has been reviewed and is approved for publication.


DONALD F. NEIDIG
Contract Manager


STEPHEN L. KEIL
Branch Chief

FOR THE COMMANDER


RITA C. SAGALYN, Director
Space Physics Division

This report has been reviewed by the ESD Public Affairs Office (PA) and is releasable to the National Technical Information Service (NTIS).

Qualified requestors may obtain additional copies from the Defense Technical Information Center. All others should apply to the National Technical Information Service.

If your address has changed, or if you wish to be removed from the mailing list, or if the addressee is no longer employed by your organization, please notify AFGL/DAA, Hanscom AFB, MA 01731. This will assist us in maintaining a current mailing list.

Do not return copies of this report unless contractual obligations or notices on a specific document requires that it be returned.

Unclassified

SECURITY CLASSIFICATION OF THIS PAGE

REPORT DOCUMENTATION PAGE

1a. REPORT SECURITY CLASSIFICATION Unclassified			1b. RESTRICTIVE MARKINGS	
2a. SECURITY CLASSIFICATION AUTHORITY			3. DISTRIBUTION/AVAILABILITY OF REPORT APPROVED FOR PUBLIC RELEASE; DISTRIBUTION UNLIMITED.	
2b. DECLASSIFICATION/DOWNGRADING SCHEDULE				
4. PERFORMING ORGANIZATION REPORT NUMBER(S)			5. MONITORING ORGANIZATION REPORT NUMBER(S) AFGL-TR-86-0062	
6a. NAME OF PERFORMING ORGANIZATION University of California		6b. OFFICE SYMBOL (If applicable)		7a. NAME OF MONITORING ORGANIZATION Air Force Geophysics Laboratory
6c. ADDRESS (City, State and ZIP Code) Department of Physics Irvine, CA 92717			7b. ADDRESS (City, State and ZIP Code) Hanscom AFB Massachusetts 01731	
8a. NAME OF FUNDING/SPONSORING ORGANIZATION		8b. OFFICE SYMBOL (If applicable)		9. PROCUREMENT INSTRUMENT IDENTIFICATION NUMBER F19628-85-K-0006
8c. ADDRESS (City, State and ZIP Code)			10. SOURCE OF FUNDING NOS.	
			PROGRAM ELEMENT NO.	PROJECT NO.
			61102F	2311
11. TITLE (Include Security Classification) Dynamic Formation of Stressed Coronal Magnetic Fields			TASK NO.	WORK UNIT NO.
			G3	DH
12. PERSONAL AUTHOR(S) R. S. Steinolfson*				
13a. TYPE OF REPORT Final Report		13b. TIME COVERED FROM 11/2/84 TO 2/2/86		14. DATE OF REPORT (Yr., Mo., Day) February 1986
15. PAGE COUNT 22				
16. SUPPLEMENTARY NOTATION * Present Address: IFS, University of Texas, Austin, TX 78712				
17. COSATI CODES			18. SUBJECT TERMS (Continue on reverse if necessary and identify by block number)	
FIELD	GROUP	SUB GR	SUN: Magnetic Fields, Active-Region Evolution	
19. ABSTRACT (Continue on reverse if necessary and identify by block number.) Magnetic fields in the quiescent solar corona usually remain connected to photospheric (subcoronal) fields. Since the ratio between the plasma and magnetic pressures satisfies $\beta \ll 1$ below the corona, the frozen-in field in this high inertia region is easily moved about by the continual motion of the photospheric plasma. In the corona, however, $\beta \leq 0.1$ and magnetic effects dominate. We have simulated the response of coronal fields to photospheric motion by subjecting a coronal magnetic cylinder, with an initially uniform axial field, to a radially varying twist at the end plates. Azimuthal symmetry is assumed, and the time-dependent MHD equations are solved numerically for a specified end-plate rotation.				
20. DISTRIBUTION/AVAILABILITY OF ABSTRACT UNCLASSIFIED UNLIMITED <input type="checkbox"/> SAME AS RPT <input checked="" type="checkbox"/> EXOTIC USERS <input type="checkbox"/>			21. ABSTRACT SECURITY CLASSIFICATION UNCLASSIFIED	
22a. NAME OF RESPONSIBLE INDIVIDUAL Donald F. Neidig			22b. TELEPHONE NUMBER (Include Area Code) 505-434-1390	22c. OFFICE SYMBOL AFGL/PHS

TABLE OF CONTENTS

INTRODUCTION	1
MODEL	2
SOLUTION PROCEDURE	5
NUMERICAL RESULTS	6
SUMMARY	8
REFERENCES	11

Accession For	
NTIS CRA&I	<input checked="" type="checkbox"/>
DTIC TAB	<input type="checkbox"/>
Unannounced	<input type="checkbox"/>
Justification	
By	
Distribution /	
Availability Codes	
Dist	Avail and/or Special
A-1	



Introduction

The structure and activity of the solar atmosphere are dominated by magnetic fields. These fields, arising from sources beneath the photosphere, channel the solar wind in coronal holes and confine the high-pressure plasma in active regions.

Of particular interest is the ability of stressed magnetic fields, usually with both ends (foot points) embedded in opposite polarity regions on the solar surface, to store significant amounts of energy. The ground state of a magnetic configuration coexisting with a highly conducting plasma is one in which no plasma currents are flowing. When currents are driven through the field/plasma structure, due to relative motions of the field sources or to voltage differences between the foot points, the magnetic energy increases.

The stored magnetic energy in active regions comprises the preflare state (Van Hoven et al. 1980). The excess (non-potential) energy in this state must be sufficient to provide the energetic-particle, flow, and thermal outputs of the flare. Using numerical codes, we compute the structure and excess energy content of the coronal magnetic field in the preflare state when the current is generated by a twisting of the field foot-points.

As stated in the proposal, the objectives we hoped to accomplish with this funding were: (a) "to complete development and check-out of the numerical code" and (b) "to conduct, at least, preliminary studies of the magnetic energy build-up due to photospheric motion." We were successful in these efforts and, in the remainder of this report, will discuss some specifics of

code development and the preliminary results.

Model

We simulate the field evolution of the magnetic loop using cylindrical (r, θ, z) geometry. This is a reasonable approximation for a narrow loop (Van Hoven 1981). We take all variables to be independent of the θ -direction so that the solution is confined to the r - z plane. We further assume that the atmosphere is initially in static equilibrium with an embedded, axial, current-free, magnetic field, that gravitational forces can be neglected when compared to the dominant magnetic forces, and that the density does not change with time. Gravity would obviously influence the evolution of the field through its effect on the dynamics. Compressibility should be relatively unimportant, at least during the early stages when the evolution is comparatively slow. Both of these quantities can be included at a later phase of this study. We do not believe, however, that either gravity or compressibility will significantly modify the basic phenomena we are investigating; namely, the build-up of magnetic energy and shear and the possibility of field reversal. The plasma β is assumed to be small enough that the pressure-gradient forces can be neglected. For this model, the single-fluid MHD equations to be solved can be written in cgs units as

$$\rho \frac{d\vec{v}}{dt} - \nabla \cdot \vec{v} \vec{v} = \frac{1}{c} \vec{j} \times \vec{B} \quad (1)$$

$$\frac{\partial \vec{B}}{\partial t} = \nabla \times \left(\vec{v} \times \vec{B} - \frac{c^2 \eta}{4\pi} \nabla \times \vec{B} \right), \quad (2)$$

along with the auxiliary equations

$$\vec{J} = \frac{c}{4\pi} \nabla \times \vec{B}, \quad \nabla \cdot \vec{v} = \nabla \cdot \vec{B} = 0.$$

The total derivative is represented by d/dt , \vec{v} is the fluid velocity, \vec{B} the magnetic field, and \vec{J} the current density. The constants are the resistivity η , the speed of light c , the density ρ , and the viscous coefficient ν . The viscosity is introduced for numerical stability reasons and to accelerate the relaxation to a static, non-potential equilibrium configuration.

The magnetic field is written as

$$\vec{B} = \frac{1}{r} \hat{e}_\theta \times \nabla \Psi + B_\theta \hat{e}_\theta + B_0 \hat{e}_z$$

where B_0 is the initial, spatially constant, axial field. The radial and axial components are then given in terms of the magnetic potential $\Psi(r, z)$; i.e.,

$$B_r = \frac{1}{r} \frac{\partial \Psi}{\partial z}, \quad B_z = B_0 - \frac{1}{r} \frac{\partial \Psi}{\partial r}.$$

Equations (1) and (2) are made dimensionless in terms of a distance a , the hydromagnetic time τ_h and velocity a/τ_h , the initial magnetic field B_0 and the density ρ . The distance a is taken to be the total radial extent of the photospheric motion in the model (this will become clear later). The three time scales in the problem are the hydromagnetic, resistive, and viscous times given by

$$\tau_h = \frac{a\sqrt{4\pi\rho_\infty}}{B_0} , \quad \tau_r = \frac{4\pi a^2}{c^2 \eta} , \quad \tau_v = \frac{a^2 \rho_\infty}{\nu} .$$

These time scales give rise to two important parameters; the Lundquist number $S = \tau_r/\tau_h$ and a viscous number $R = \tau_v/\tau_h$.

The dimensionless versions of equations (1) and (2) can then be written in component form [$\vec{v} = (v_r, v_\theta, v_z) \propto (u, v, w)$] as

$$\begin{aligned} \rho \frac{\partial u}{\partial t} - \frac{1}{R} \nabla^2 u = & - \frac{1}{r^2} \left(\frac{\partial^2 \Psi}{\partial z^2} + \frac{\partial^2 \Psi}{\partial r^2} - \frac{1}{r} \frac{\partial \Psi}{\partial r} \right) \left(\frac{\partial \Psi}{\partial r} - r B_0 \right) \\ & - \left(\frac{\partial B_\theta}{\partial r} + \frac{B_\theta}{r} \right) B_\theta , \end{aligned} \quad (3)$$

$$\rho \frac{\partial v}{\partial t} - \frac{1}{R} \nabla^2 v = \frac{1}{r} \left(\frac{\partial B_\theta}{\partial r} + \frac{B_\theta}{r} \right) \frac{\partial \Psi}{\partial z} - \frac{1}{r} \frac{\partial B_\theta}{\partial z} \left(\frac{\partial \Psi}{\partial r} - r B_0 \right) , \quad (4)$$

$$\rho \frac{\partial w}{\partial t} - \frac{1}{R} \nabla^2 w = - B_\theta \frac{\partial B_\theta}{\partial z} - \frac{1}{r^2} \left[\frac{\partial^2 \Psi}{\partial r^2} + \frac{\partial^2 \Psi}{\partial z^2} - \frac{1}{r} \frac{\partial \Psi}{\partial r} \right] \frac{\partial \Psi}{\partial z} , \quad (5)$$

$$\frac{\partial \Psi}{\partial t} - \frac{1}{S} \nabla^2 \Psi = - w \frac{\partial \Psi}{\partial z} + r u B_0 - u \frac{\partial \Psi}{\partial r} , \quad (6)$$

$$\begin{aligned} \frac{\partial B_\theta}{\partial t} - \frac{1}{S} \left(\frac{\partial^2 B_\theta}{\partial r^2} + \frac{\partial^2 B_\theta}{\partial z^2} + \frac{1}{r} \frac{\partial B_\theta}{\partial r} - \frac{B_\theta}{r^2} \right) = & B_0 \frac{\partial v}{\partial z} - \frac{1}{r} \frac{\partial \Psi}{\partial r} \frac{\partial v}{\partial z} \\ & - w \frac{\partial B_\theta}{\partial z} - B_\theta \frac{\partial w}{\partial z} - u \frac{\partial B_\theta}{\partial r} - B_\theta \frac{\partial u}{\partial r} + \frac{\partial \Psi}{\partial z} \left(\frac{1}{r} \frac{\partial v}{\partial r} - \frac{v}{r^2} \right) , \end{aligned} \quad (7)$$

where a simplified form of

$$\nabla^2 \rightarrow \frac{1}{r} \frac{\partial}{\partial r} \left(r \frac{\partial}{\partial r} \right) + \frac{\partial^2}{\partial z^2}$$

has been used in (3) - (6) to provide dissipative relaxation.

The advection terms have been dropped in view of the small

velocities ($\sim 10^{-2}a/\tau_h$) applied.

Solution Procedure

The method of excitation used to simulate the photospheric input is to rotate the ends of a cylindrical loop (contained within the initial axial field) at a radially-dependent rate out to some maximum radius a beyond which the ends remain fixed. The time dependence of the rotation can have any specified form; i.e., the rotation can be increased with time to some maximum and then either remain constant or be decreased to zero; the rotation can remain fixed at a given value throughout the computation; or, alternatively, it can be reduced to zero after a given time interval, etc. Throughout these preliminary computations the rotation rate has been held fixed at a specified level during the simulation.

The radial variation of the input rotation that we have used to obtain the results presented herein is as shown on the left edge of Figure 1. The azimuthal velocity increases linearly with radius (as in rigid rotation) from zero at the cylinder center to a maximum (10 km s^{-1}) at $r = 0.8a$, after which it linearly decreases to zero at $r = a$.

The remaining quantities to be specified are the boundary conditions. These are trivial at the loop axis. Linear extrapolation is used at the maximum radius, although this is so large the variables do not undergo much change there. For simplicity in these initial computations, the ends of the loop are assumed to be twisted identically in opposite directions so

the axial mid-point becomes a plane of symmetry. Consequently, at the the mid-point (considered to simulate the loop top), Ψ, B_θ, u , and v are symmetric and $w = 0$. At the loop base, v and B_θ are given by the specified rotation, $u = \Psi = 0$, and w is linearly extrapolated.

Equations (3) - (7) are now solved numerically by first solving equation (6) implicitly for Ψ using velocities from the previous time step. The remaining equations are then solved using the leapfrog Dufort-Frankel scheme (Peyret and Taylor 1983). The leapfrog method was initially used on all equations, but numerical instabilities developed in Ψ .

Numerical Results

The physical values used for the results presented below are as follows: $a = 10^7$ cm, $B_0 = 10.5$ G, $\rho_\infty = n_\infty m_p$ with m_p = proton mass and $n_\infty = 10^9$ cm $^{-3}$, and $T_\infty = 1.6 \times 10^6$ °K. These parameters provide $\beta = 0.1$. The Lundquist and viscous numbers are taken to be 10^3 . Some features of the solution after 12,000 time cycles or approximately 260 hydromagnetic times are presented in Figures 1, 2, and 3.

Three field lines are shown in Figure 1 as they would appear in projection onto the r - z plane when the cylinder is viewed from the side. Two of the field lines start at the base within the region of rotation ($r < a$) and one (the short dashed curve) starts beyond it. All three are initiated at the base in the plot on a vertical axis (from the illustrated viewpoint) taken to be at $\theta = 0^\circ$. The total rotation or twist of each of the field

lines between the base and mid-point is indicated on the figure.

The field line starting near the maximum rotation rate at the base naturally has the largest amount of twist. Interestingly, however, more than half of the twist for the field line (122°) occurs within approximately 0.2 dimensionless units (z/a) of the base. The inner field line has very little twist, while the outer one rotates almost uniformly along its entire length.

The radial variation of the magnetic field components are plotted in Figure 2 at the axial location ($z \approx 0.8a$) indicated on Figure 1. The most interesting feature here is the concentration of the axial field near the loop axis. This is seen in all simulations, for various parameters, that have been conducted to date. The radial component has a maximum near the axis, and the azimuthal component peaks somewhat further out.

The axial run of the field components are shown in Figure 3 at a radial location ($r \approx 0.8a$) near the region of maximum rotation at the base (see Figure 1). All components are largest near the base. The axial currents generated by the base rotation tend to keep the azimuthal field almost constant along the cylinder.

A few field lines from an analytic solution (Zweibel and Boozer 1985) to a problem which is similar to that we have considered are given in Figure 4. Only the radial and axial field components are shown in this presentation in contrast to the results in Figure 1, in which the azimuthal component was also considered in order to give the true projection view.

Although Zweibel and Boozer (1985) had to make some additional approximations (e.g., long and narrow cylinder) to obtain the analytic result, it is clear that our results and theirs are qualitatively similar. Both show that most of the radial curvature occurs near the base (left edge in Figure 4), and both exhibit a concentration of field near the cylinder axis.

The initial magnetic energy contained within the cylinder in which the solution was computed was 1.11×10^{23} ergs. The energy when the solution was terminated was 1.29×10^{24} ergs, representing an increase of more than an order of magnitude.

Summary

This research has demonstrated that there are three characteristic features which occur in initially axial magnetic fields as a result of twist at the end plates of a cylindrical portion of this field. These appear to be very general characteristics since they occurred to a varying extent in all simulations conducted to date. First of all, most of the twist occurs near the cylinder base. The rotating end plates also tend to concentrate the magnetic field near the cylinder axis over most of the tube. Finally, the largest radial curvature concentrates near the base in conjunction with the inward pinching of the field lines.

Results of this research program have been presented at the annual meeting of the Division of Plasma Physics of the American Physical Society (Steinolfson and Schnack 1985). We also intend to present some of this work at the summer meeting of the

American Astronomical Society, and plan that it will form part of the content of a longer paper which is in preparation.

References

- Peyret, R., and Taylor, T. D., 1983, Computational Methods for Fluid Flow, Springer-Verlag, pp. 44-45.
- Steinolfson, R. S., and Schnack, D. D., 1985, Bull. Am. Phys. Soc. 30, 1470.
- Van Hoven, G., et al., 1980, "The Preflare State", in Solar Flares (P. A. Sturrock, ed.), Univ. of Colo. Press, pp. 17-81.
- Van Hoven, G., 1981, "Simple Loop Flares: Magnetic Instabilities", in Solar Flare Magnetohydrodynamics (E. R. Priest, ed.), Gordon and Breach, pp. 217-275.
- Zweibel, E., and Boozer, A., 1985, Astrophys. J. 295, 642.

Figure Captions

Figure 1. The rotation velocity is sketched on the left. Three field lines are shown as they would appear in projection when the cylinder is viewed from the side. All of the field lines start in a vertical plane ($\theta = 0^\circ$) at the base. The inner field line (—) has very little twist. The center line (— —) has the most twist, but the majority of it occurs near the base. The outer field line (- - -) is twisted almost uniformly along its entire length.

Figure 2. Radial profiles of the magnetic field components at the axial location indicated on Figure 1. The axial and radial components concentrate near the axis.

Figure 3. Axial profiles of the magnetic field components at the radial location indicated in Figure 1. The radial and axial components are largest near the base, while the azimuthal component only varies by a small amount over most of the cylinder length.

Figure 4. Flux-surface contours from Zweibel and Boozer (1985). The present numerical computations agree with this analytic result.

(Fig. 2 plot)

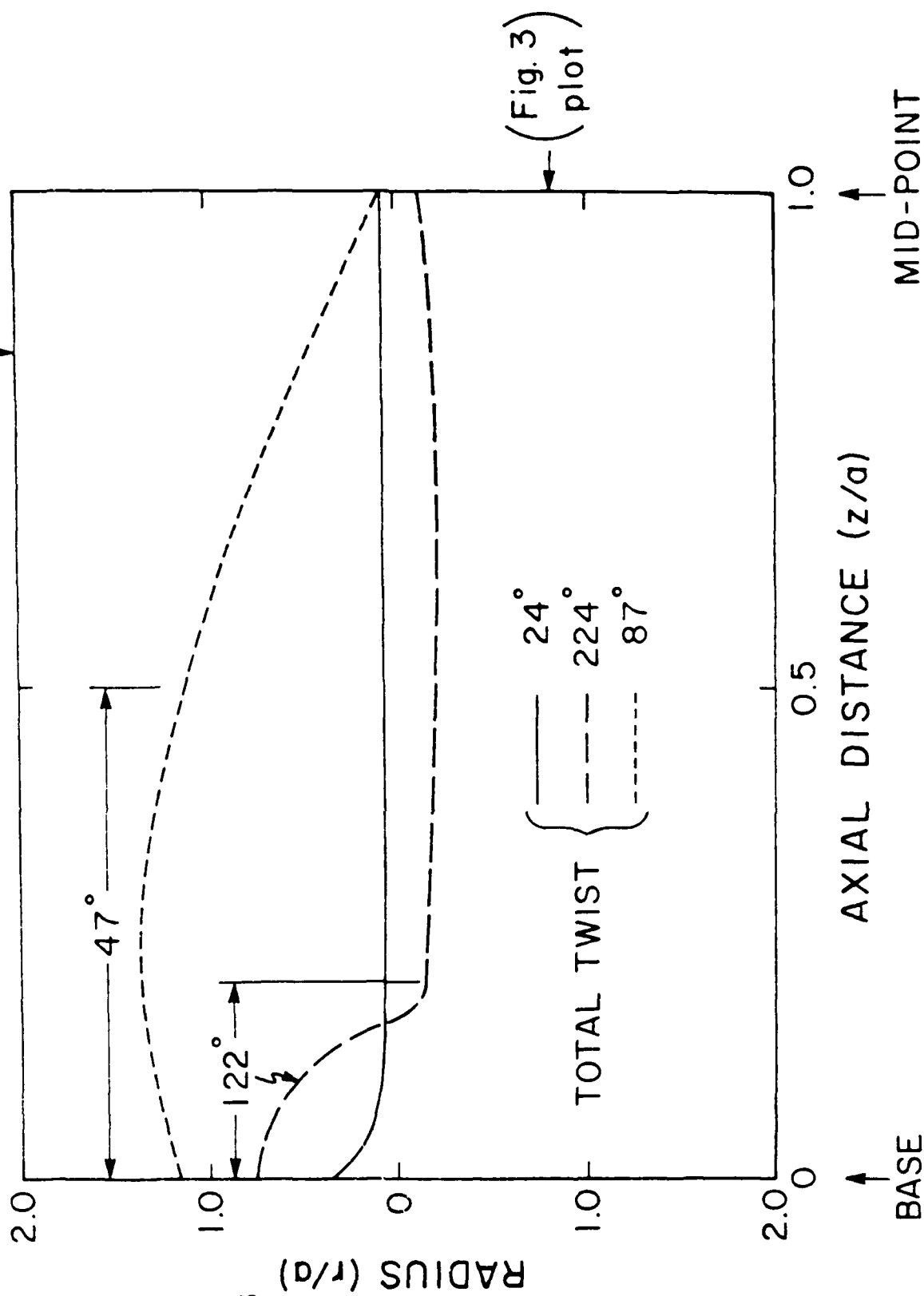
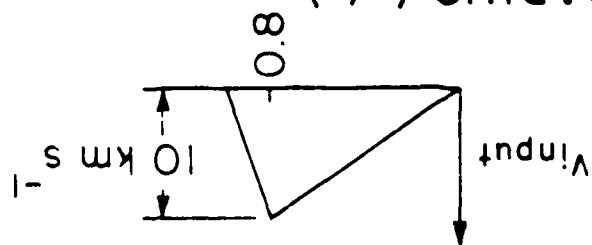


Figure 1



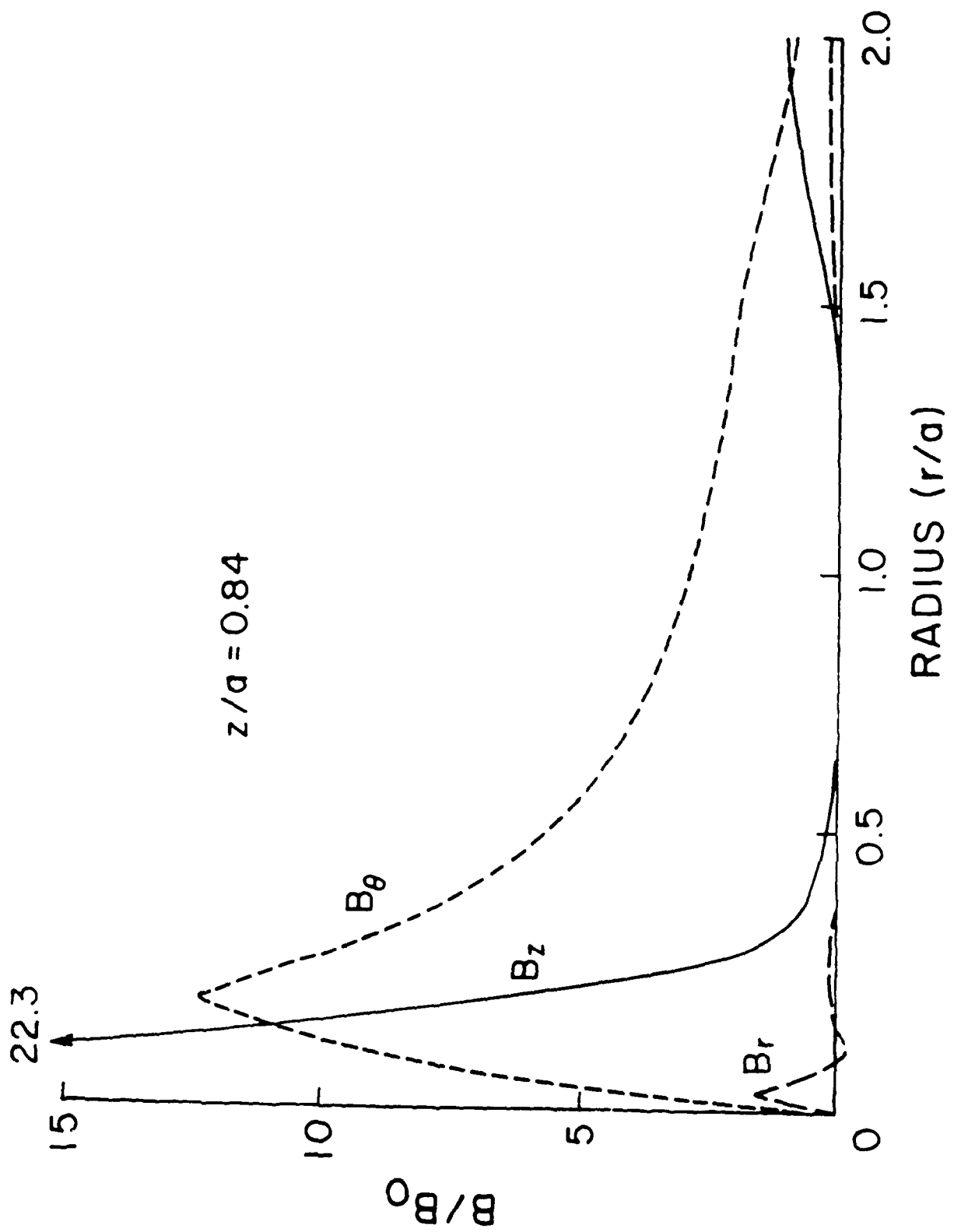


Figure 2

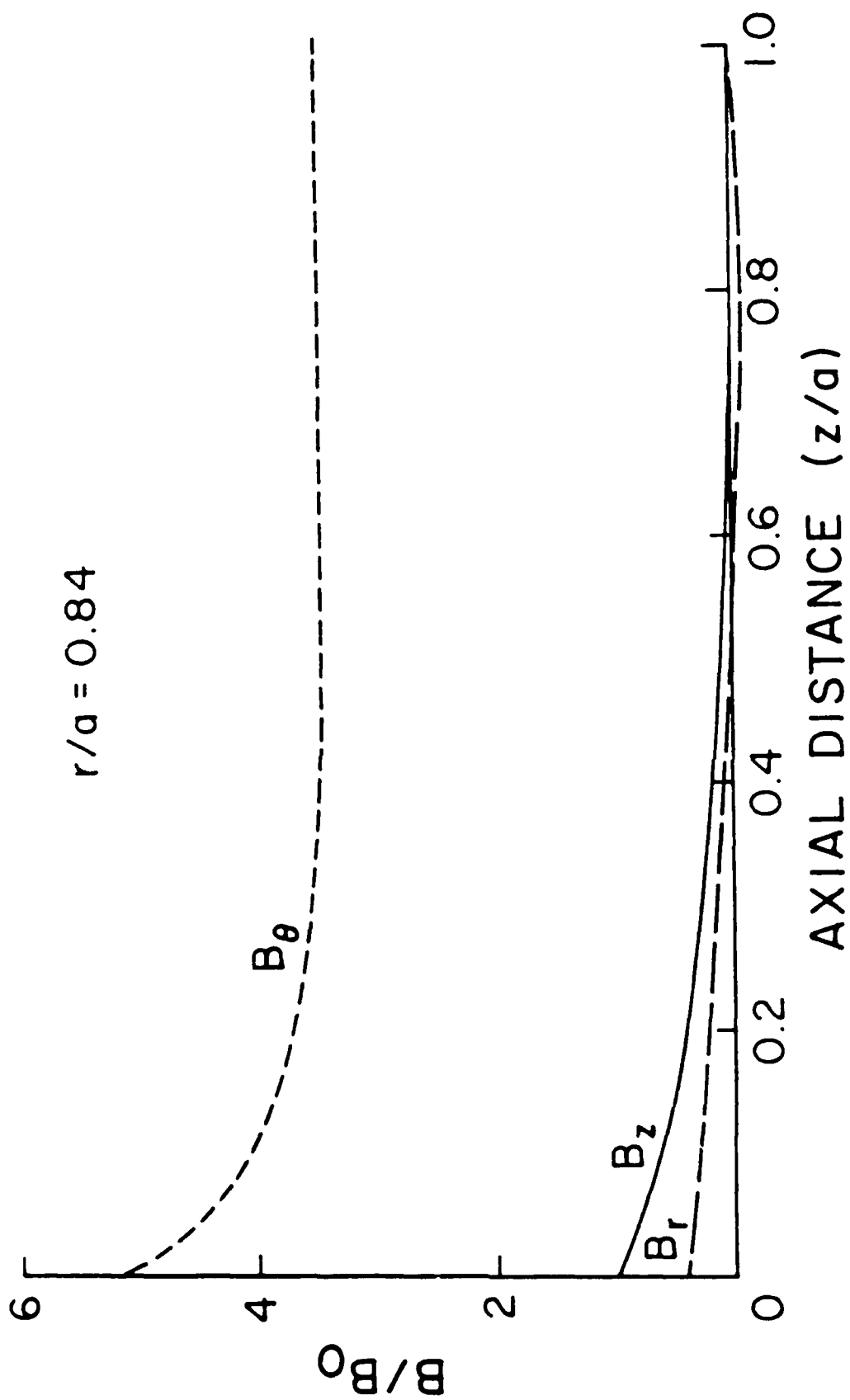
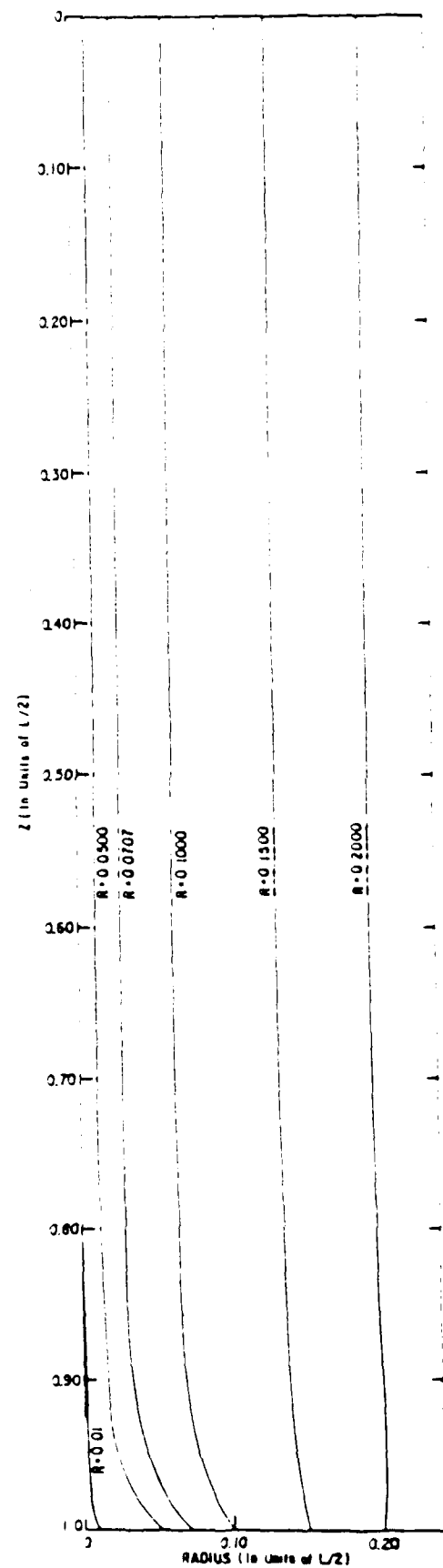


Figure 3



[Fig. 1 from Zweibel and Boozer (1985)]

FIGURE 4

END

DTIC

8-86